small NANO MICRO

Nanoparticle delivery

Nanofountain-Probe-Based High-Resolution Patterning and Single-Cell Injection of Functionalized Nanodiamonds**

Owen Loh, Robert Lam, Mark Chen, Nicolaie Moldovan, Houjin Huang, Dean Ho, and Horacio D. Espinosa**

***N**anodiamonds are rapidly emerging as promising carriers for next-generation therapeutics and drug delivery. However, developing future nanoscale devices and arrays that harness these nanoparticles will require unrealized spatial control. Furthermore, single-cell in vitro transfection methods lack an instrument that simultaneously offers the advantages of having nanoscale dimensions and control and continuous delivery via microfluidic components. To address this, two modes of controlled delivery of functionalized diamond nanoparticles are demonstrated using a broadly applicable nanofountain probe, a tool for direct-write nanopatterning with sub-100-nm resolution and direct in vitro single-cell injection. This study demonstrates the versatility of the nanofountain probe as a tool for high-fidelity delivery of functionalized nanodiamonds and other agents in nanomanufacturing and single-cell biological studies. These initial demonstrations of controlled delivery open the door to future studies examining the nanofountain probe's potential in delivering specific doses of DNA, viruses, and other therapeutically relevant biomolecules.*

Keywords:
- arrays
- drug delivery
- nanodiamonds
- nanoparticles
- nanopatterning

1. Introduction

Nanoparticles have proven to be highly efficient carriers of biological agents. Examples include the use of nanoparticle–agent conjugates for gene regulation[1,2] and delivery of a variety of therapeutics.[3–7] Their potential impact on drug delivery is emergent in early experimental results showing moderated drug activity through controlled release from the nanoparticles.[3,5,8] Studies also demonstrate the innate biocompatibility of the nanoparticles themselves (e.g., diamond[3,9–12] and gold[13,14]). To fully leverage this potential within devices and methods, a greater degree of control over nanoparticle placement is desirable. Toward this goal, we present a nanofountain probe (NFP) for high-resolution delivery of functionalized nanoparticles across multiple cell lines. As a case study, we demonstrate the ability of the NFP to pattern dot arrays of drug-coated diamond nanoparticles with sub-100-nm resolution for future hybrid devices that require great spatial fidelity, as well as in vitro single-cell injection of fluorescently labeled diamond nanoparticles.

[*] Prof. H. D. Espinosa, O. Loh, R. Lam, H. Huang, N. Moldovan
Department of Mechanical Engineering
Northwestern University
2145 Sheridan Rd.
Evanston, IL 60208-3111 (USA)
E-mail: espinosa@northwestern.edu
Prof. D. Ho
Depts. of Mechanical Engineering and Biomedical Engineering
Northwestern University
2145 Sheridan Rd.
Evanston, IL 60208-3111 (USA)
E-mail: d-ho@northwestern.edu
M. Chen
Department of Chemistry
Northwestern University
2145 Sheridan Rd.
Evanston, IL 60208-3113 (USA)

[**] O. L. and R. L. contributed equally to this work.

Supporting Information is available on the WWW under http://www.small-journal.com or from the author.

DOI: 10.1002/smll.200900361

Diamond nanoparticles, also referred to as nanodiamonds (NDs) or detonation diamonds after their method of production, garner great attention in biomedical fields for their unique properties. These include an innate biocompatibility,[3,9–12] precise particle distributions,[15] an extreme surface area-to-volume ratio,[16] a near-spherical aspect ratio, and an easily-adaptable carbon surface for bioagent attachment.[17–19] NDs have been functionalized with a range of therapeutics, proteins, antibodies, DNA, and other assorted biological agents.[3,17,20–24] For example, NDs were coated with doxorubicin hydrochloride (DOX), a commonly-used chemotherapeutic agent, through physisorption.[3] The drug-coated NDs were then embedded in polymer microfilms, where they demonstrated a constant moderate rate of drug elution over a period of months.[8]

While inherently challenging, the ability to pattern functionalized NDs is desirable in creating the next generation of biological devices with precise spatial and temporal tuning of multiple drug release, as well as single-cell in vitro studies. Currently, these are generally limited to the use of serial dilution of ND solutions and deposition of continuous ND films.[3,8,20,25] Some degree of spatial control has been achieved by patterning NDs using inkjet printing techniques. For example, NDs in solution were printed with minimum feature sizes on the order of 100 μm.[26,27] However, this resolution does not approach the ultimate subcellular control desired in nanomaterial-mediated drug delivery studies and devices.

Though not demonstrated for NDs, a number of direct transfer and directed self-assembly techniques have been used to pattern other types of nanoparticles.[28] Some examples of direct-transfer deposition include dip-pen nanolithography,[29–31] NFPs,[32] microcontact printing,[33–35] electrohydrodynamic[36] and inkjet printing,[37] nanopipettes,[38,39] microarrayers,[40] surface patterning tools,[41] and various forms of lithography.[42,43] For directed self-assembly, chemical templates are patterned upon which nanoparticles in solution selectively adhere. Techniques used to create these chemical templates include dip-pen nanolithography,[44–47] lithography,[48] and microcontact printing.[49,50] While sub-100-nm features are possible, the strong nanoparticle–substrate binding required for well-defined self-assembled features may not be desirable in cases where the drug or other agent must be released. Furthermore, while a variety of substrate–nanoparticle conjugations have been developed for directed assembly, the possibilities may be somewhat more limited for agent-coated nanoparticles.

Beyond precision delivery for dosing and nanomanufacturing, continuous nanoscale transfections without supplemental chemical procedures have often been limiting factors in single-cell studies. Common methods of transfection include carrier-mediated transfer,[51] biological,[52,53] chemical,[54,55] or electrical plasma membrane permeabilization,[56] and direct injection.[57–59] Each of these methods has well-documented advantages and disadvantages.[58,60] For single-cell studies in particular, direct injection methods are attractive due to their precision targeting and compatibility with virtually any biologically relevant agent and cell type. However, there are drawbacks to traditional cellular injection methods, such as the need for specialized equipment, arduous and lengthy training, and cellular damage caused by the incorporation of a relatively large micropipette needle.[58,60] To reduce invasiveness, several methods employing nanoscale tools have been developed. These include nanoneedles,[61–64] microcantilevers,[65–68] optical nanoinjection,[69] and electrochemical attosyringes.[70] In the case of nanoneedles and microcantilevers, the material to be injected is immobilized on the exterior surface of the probe. Therefore, it must remain bound during the injection process and then subsequently released within the cell. This generally requires specialized chemical modification of the probe surface,[62,64] a process that can be complicated for agent-coated nanoparticles.

As an alternative to the above patterning and direct-injection methods, we take advantage of the NFP's[71–73] unique design to achieve both sub-100-nm patterning and direct in vitro injection of functionalized nanoparticles. The NFP is an atomic force microscope (AFM)-based delivery probe (Figure 1). Liquid molecular "inks" stored in an on-chip reservoir are fed through integrated microchannels to apertured dispensing tips (Figure 1a, inset) by capillary action. This allows continuous delivery either to a substrate for direct-write nanopatterning (Figure 1b), or to a cell for in vitro injection (Figure 1c). In the case of direct-write nanopatterning, the sharp apertured tip geometry allows for a unique combination of resolution and generality in its ability to pattern a broad range of organic and inorganic molecules and nanoparticle solutions. Past demonstrations of direct-write nanopatterning include proteins[74] and DNA[75] in buffer solution, gold nanoparticles in aqueous suspension,[32] and thiols.[71,73] For direct injection, the sharp core tip reduces damage to the cell while the outer shell guides the molecules directly to the point of injection. Furthermore, under control of the AFM,[63,67] a ubiquitous research tool, accurate NFP tip placement and real-time force measurements are achievable with respective resolutions of nanometers and nanoNewtons.

In this article we demonstrate the utility of the NFP in two methods of single-cell interrogation and nanomanufacturing using DOX-ND conjugates: direct-write nanopatterning of nanoscale dot arrays and targeted direct in vitro injection. In these demonstrations we emphasize the NFP as an enabling technology for future single-cell nanoparticle-mediated drug delivery studies and manufacturing of nanoparticle-based

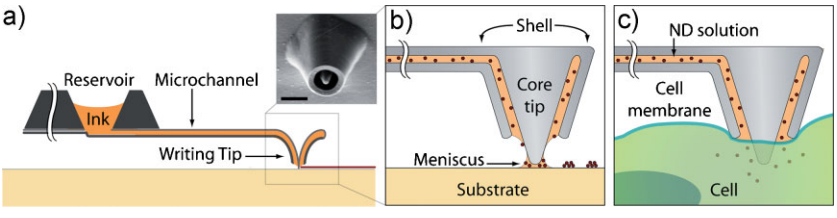

Figure 1. Schematic of ND ink delivery using the NFP. a) Liquid ink is stored in an on-chip reservoir and fed through enclosed microchannels to apertured writing tips by capillarity. The inset shows a scanning electrom microscopy (SEM) image of an apertured tip (scale bar: 2 μm). b) For direct-write nanopatterning, the tip is brought into contact with the substrate where an ink meniscus forms. c) For in vitro cellular injection, the tip is introduced to the cell membrane with a prescribed insertion force.

biological devices. The demonstrated degree of control allows fundamental investigations on a single-cell level, and further provides a platform by which to fabricate precisely tuned drug delivery devices using multiprobe arrays[71–73] for parallel nanomanufacturing.

2. Results and Discussion

2.1. Patterning Functionalized Nanodiamonds

The ability of the NFP to precisely place repeatable doses was first assessed by patterning dot arrays of drug-coated NDs (drug-NDs). NDs were coated with DOX, a commonly used chemotherapeutic agent that acts through intercalation with a cell's DNA, causing fragmentation and eventual apoptosis. Dot arrays of drug-NDs were patterned directly on glass substrates using the NFP (Figure 2). To create each dot, the NFP was brought into contact with the substrate for a prescribed dwell time, then lifted and translated to the next point in the array at a rate of 100 $\mu m\,s^{-1}$. While DOX was used herein as a case study, we emphasize the broader utility of the technique as NDs have proven capable of carrying a variety of drugs and bioagents.[3,17,20–24]

To test patterning resolution and repeatability for dose control, drug-ND dot arrays were created and the consistency of features for a given dwell time assessed. Figure 2a shows a representative array patterned with 4 s dwell times (see Supporting Information for further examples). Feature size (dot diameter (Figure 2b–e) and height (Figure 2f)) were measured for dwell times ranging from 1.5 to 5 s. As shown in Figure 2g, both dot diameter and height show little spread for a given dwell time, and strong linear dependence on the square root of the dwell time. This allows precise dose control through selection of dwell time. Individual dot features were well-defined and densely packed (Figure 2d inset). The intrinsic fluorescence[76,77] of DOX was used as an initial confirmation of the presence of drug within the patterned features (Figure 2h,i). Combined with the excellent spatial positioning resolution of

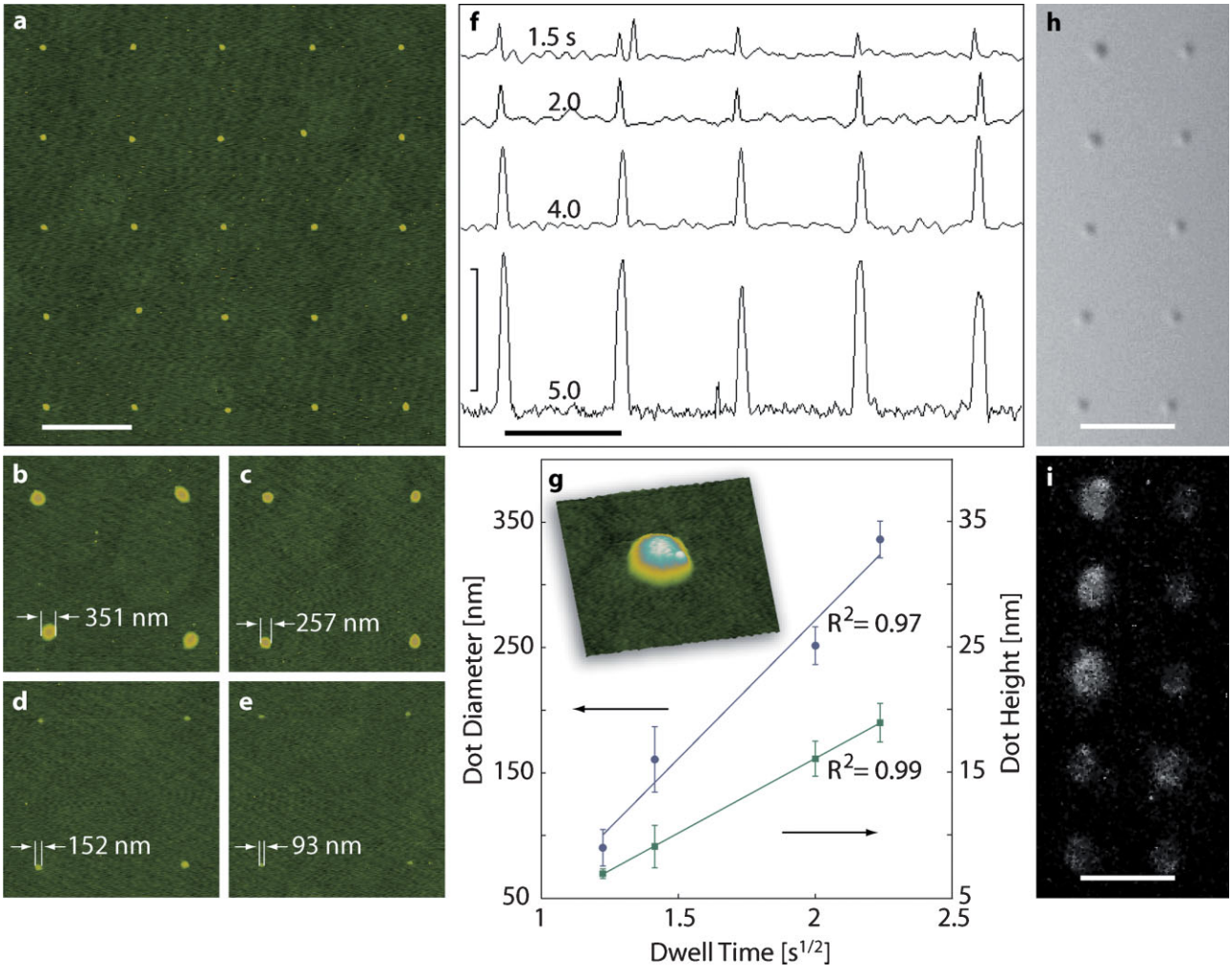

Figure 2. Patterning functionalized NDs. a) Tapping-mode AFM image of a representative dot array of drug-NDs patterned with 4 s dwell times at 28% relative humidity. Scale bar: 4 μm. b–e) Tapping-mode AFM images of drug-ND dots patterned with varying dwell times of 5 (b), 4 (c), 2 (d), and 1.5 s (e) at 28% relative humidity. Diameters are measured from full width at half maximum. f) Cross sections of dot arrays for different dwell times (scale bar: 4 μm, height scale 20 nm). g) Dot feature size as a function of square-root dwell time. Lines are a linear fit. The inset is a 1-μm scan of a single dot feature showing its densely packed structure. h,i) Bright field (h) and epi-fluorescence (i) images of a dot array confirming DOX presence in patterned features. Scale bars: 4 μm.

the AFM, the NFP can thus be used to control local dosing both through patterned feature size and pitch.

NFP-based drug-ND patterning was tested using both water and dimethyl sulfoxide (DMSO) solvents, yielding similar results. In previous applications of the NFP, it was shown that the size of the meniscus formed at the tip of the NFP (Figure 1b), and thus the feature size, depends upon the contact angle between the liquid and substrate.[32,74] Here the contact angle between the drug-ND solution and glass substrate was measured to be $29^\circ \pm 2^\circ$ for the DMSO solution versus $27^\circ \pm 4^\circ$ for the aqueous solution. Thus it is not surprising to find similar dwell time–feature size dependence.

Beyond demonstration of the ability to precisely place a prescribed dose of drug-NDs, the preserved activity of the drug was tested. A 36×36 μm area dot array was first patterned on a glass coverslip. Murine macrophages were plated on the patterned substrate and incubated for 24 h. A terminal deoxynucleotidyl transferase dUTP nick end labeling (TUNEL) assay[78] was then performed to detect DNA fragmentation and apoptosis, the key inducing mechanism of DOX. Figure 3a and b show the negative and positive controls of the TUNEL assay, respectively, with the positive control exhibiting diminished population with approximately 50% of the remaining cells being TUNEL-positive. The negative control shows minimal sign of apoptosis and significantly greater confluency. Like the positive control, the patterned sample (Figure 3c) shows a significant fraction of TUNEL-positive cells and diminished population relative to the positive control, strongly suggesting that the DOX remains active upon patterning, attesting to the inviolate NFP deposition process. Given the 100-nm ND patterning resolution, we emphasize here the demonstration of the NFP as an enabling technology for future studies and the nanomanufacturing of intelligent drug release devices.

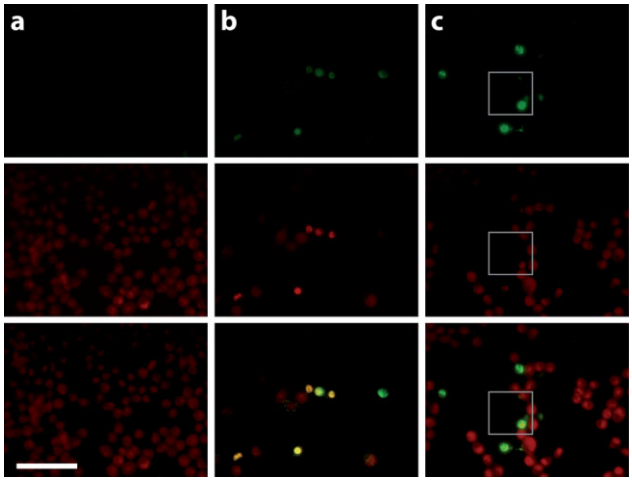

Figure 3. TUNEL assay testing preserved activity of patterned DOX-NDs. TUNEL, counterstain, and overlaid images for each case are shown in the top, middle, and bottom rows respectively. a) Negative control shows no TUNEL-positive cells. Scale bar: 50 μm (same in all images). b) Positive control shows approximately 50% TUNEL-positive cells and reduced confluency. c) Test sample with 1296 μm^2 patterned region boxed. Significant numbers of TUNEL-positive cells are present and population is reduced relative to negative control.

2.2. In vitro Injection of Functionalized Nanodiamonds

Beyond nanopatterning for biological studies and nanomanufacturing, the ability to directly inject doses of drug-bound nanoparticles (e.g., NDs) into cells allows further study of the response of a single cell to a given dose. Here we demonstrate the ability of the NFP to facilitate these studies. The positional accuracy and force sensitivity of the AFM, a pervasive tool in research, are leveraged to guide the NFP during targeted cell injection.

NDs were first fluorescently labeled to facilitate characterization of NFP-mediated injection. Fluorescent fluorescein isothiocyanate (FITC) poly-(L-lysine) (PLL-FITC) was physisorbed onto ND particles as previously reported.[3,20] It has been demonstrated previously that carboxyl groups on the ND surface provide a binding mechanism for non-specific adsorption for PLL-based molecules.[79–81] This bond has been established for DNA[79] and protein immobilization,[80,81] with negligible signs of deterioration within biological solutions. The binding was characterized by UV–Vis spectral analysis before and after centrifugation (Figure 4a–c). In contrast to free PLL-FITC samples (Figure 4b), the absorbance of pristine ND (Figure 4a) and ND-PLL-FITC (Figure 4c) solutions decreased significantly upon centrifugation. This indicates binding of the PLL-FITC molecules to the ND surface and subsequent pull-down with the NDs during centrifugation. High-resolution transmission electron micrographs (TEMs) of ND-PLL-FITC aggregates further confirm the assumed PLL-FITC-coated ND structure (Figure 4d). Visible atomic lattice fringes clearly differentiate the crystalline diamond and amorphous coating material assumed to be the physisorbed PLL-FITC labeling.

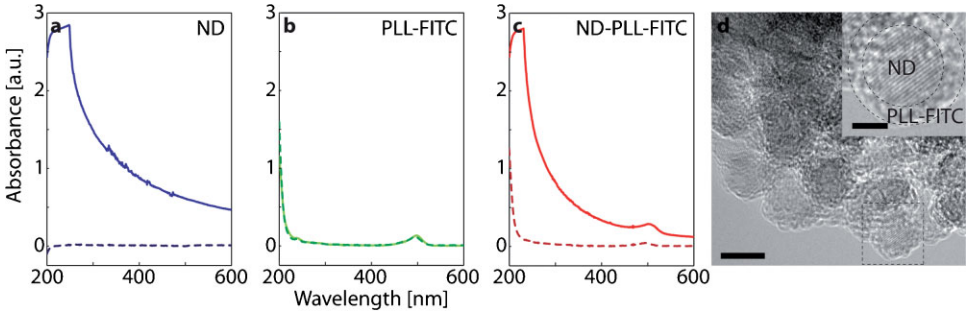

Figure 4. Characterization of fluorescently labeled NDs. a–c) UV–Vis absorption spectra for pristine ND (a), free PLL-FITC (b), and bound ND-PLL-FITC (c) solutions before (solid line) and after (dashed line) centrifugation. A significant drop in the ND-PLL-FITC signal relative to the free PLL-FITC (similar to the pure NDs) indicates strong binding. d) TEM images of ND-PLL-FITC show the lattice structure of the crystalline diamond particles coated by amorphous material. Scale bars: 5 nm, 2.5 nm in the inset.

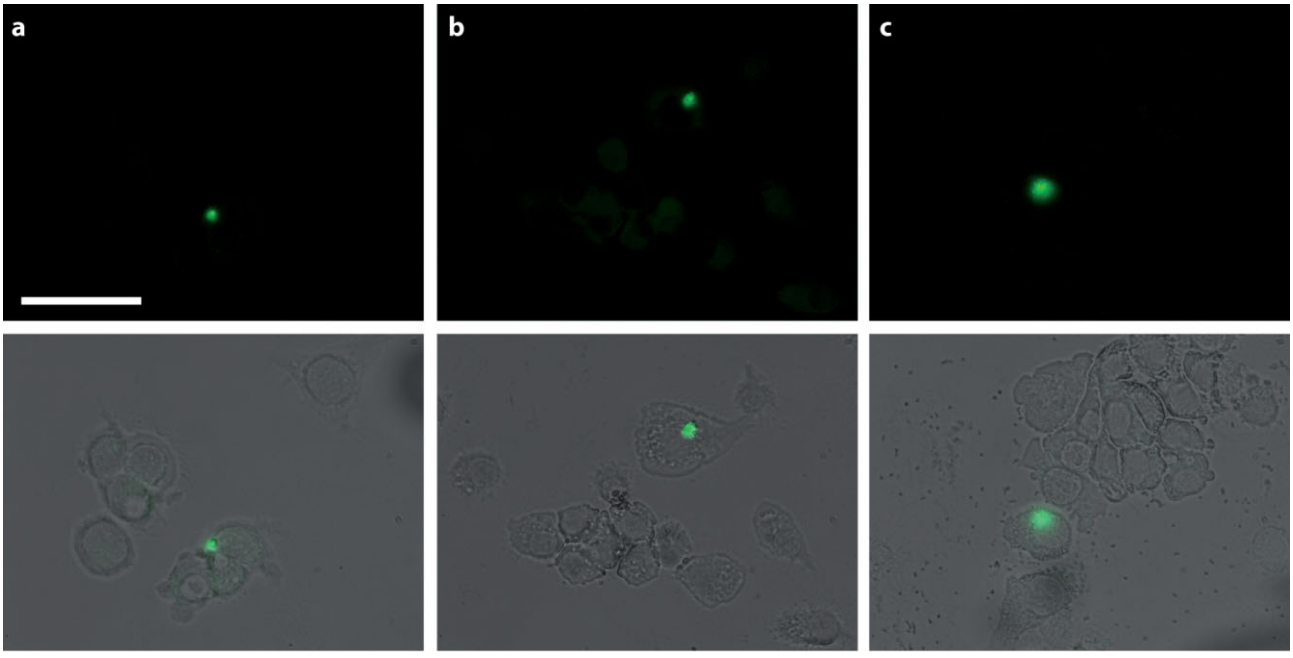

Figure 5. Epifluorescence (top row) and fluorescence-bright field overlay (bottom row) images showing targeted injection of FITC-labeled NDs into a single a) MCF-7 human breast adenocarcinoma cell, b) RAW 264.7 murine macrophage, and c) RKO colorectal carcinoma cell. Injection times were 5, 10 and 15 s, respectively. Scale bar: 50 μm.

NFP-mediated injection of the fluorescently-labeled NDs was demonstrated on multiple cell lines. Figure 5 depicts the successful injection of FITC-PLL-NDs into individual MCF-7 human breast adenocarcinoma cells, RAW 264.7 murine macrophages, and RKO colorectal carcinoma cells. The observed fluorescence is highly localized within a single cell. The well-defined fluorescent dose further suggests that the membrane was not severely damaged so as to allow the ND-PLL-FITC to quickly diffuse out into the media.

As a preliminary study, the spreading and kinetics of the injected nanoparticles were further investigated by estimating the diffusion coefficient for ND-PLL-FITC in cytoplasm using an integrative optical imaging technique.[82,83] The spread in fluorescent intensity of the injected dose in an MCF-7 cell (Figure 5a) was captured in a series of images over time (Figure 6). The intensity profile along an axis in each image was fit with a Gaussian function, and the diffusion coefficient computed as described by Nicholson and coworkers[82,83] (see Supporting Information for further description). Here a diffusion coefficient of $(11.8 \pm 0.2) \times 10^{-3}\ \mu m^2 \cdot s^{-1}$ at 25 °C was computed. This is about four times greater than that reported by Chang et al.[84] for larger fluorescent NDs ($3.1 \times 10^{-3}\ \mu m^2 \cdot s^{-1}$ for 35-nm NDs[84] versus the 4- to 10-nm NDs used herein). A greater diffusion coefficient is expected for smaller particles, as reported for a broad range of macromolecules.[82,83,85,86] Similarly, a size-dependent cellular response has also been reported.[87]

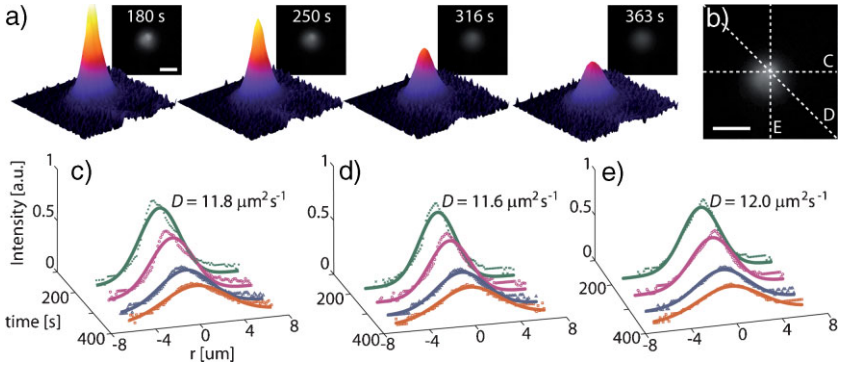

Figure 6. Characterization of ND-PLL-FITC diffusion in MCF-7 cell. a) Sequence of fluorescence images captured following ND-PLL-FITC injection. Raw image and false color 3D representations are shown (scale bar: 5 μm). b) Three axes, labeled C–E, from which fluorescence intensity profiles were extracted (scale bar: 5 μm). c–e) Fluorescence intensity profiles extracted along the three axes C–E respectively shown in (b). In each plot, the raw data and fitted Gaussian function are shown for the four images shown in (a). Green, magenta, blue, and orange represent the intensity profiles at 180, 250, 316 and 363 s, respectively.

3. Conclusions

The enabling capabilities of the NFP technology for future nanomanufacturing of drug delivery devices and single-cell nanomaterial-mediated delivery studies were demonstrated. Two methods of interrogation, direct-write patterning of drug-coated nanoparticles and direct in vitro injection of fluorescently-labeled nanoparticles, were successfully established. For nanomanufacturing, dot arrays were patterned with sub-100-nm resolution. Feature size showed a strong linear dependence on square root dwell time, enabling precise and repeatable dosing control. Preserved drug activity in the patterned arrays was also confirmed. For single-cell studies, well-defined direct injection of fluorescently-labeled NDs was

demonstrated on multiple cell lines. Since diffusion is the central mechanism of injection, prospective studies involving the delivery of controlled doses of DNA-plasmids, siRNA, viruses, and other therapeutics also have exciting implications in determining and directing single-cell response.

The apertured core–shell tip geometry of the NFP allows for a unique combination of patterning resolution and generality in its ability to pattern and deliver a range of liquid solutions. The combination of multiprobe arrays[71–73] and on-chip reservoirs for continuous ink delivery enables parallel nanomanufacturing for extended periods. Combined with the precise control of the AFM, highly-targeted in vitro injection is further possible.

Nanopatterning drug-ND conjugates affords extremely precise quantitative and positional control of dosing. It was recently shown that DOX-NDs embedded in parylene are capable of controlled drug release over a period of months.[8] These embedded microfilms are currently being pursued as implants for targeted drug delivery. An attractive enhancement would be to replace the continuous drug-ND films currently used in these devices with patterned arrays using multiple drugs. This allows high fidelity spatial tuning of dosing in intelligent devices for comprehensive treatment. Furthermore, explicit patterning control of NDs would offer avenues for the construction of novel biological nanoparticle assays[88] and immediate future nanomanufactured materials via seeding and nucleation of diamond thin film growth.[89,90]

In vitro injection of functionalized nanoparticles enables fundamental studies of nanomaterial-mediated drug delivery. To demonstrate this, an exploratory study was performed by investigating the intracellular dynamics of NDs upon nanoinjection. Important questions that remain to be investigated include fundamental explanation of internalization mechanisms and minimum dosing for desired efficacy. Towards these studies, NFP-based injections prove promising by combining the generality of micropipette systems with the reduced invasiveness of nanoscale injection tools.

Previous reports demonstrate significantly reduced cellular damage using nanoscale injection tools with tip diameters less than 400 nm.[61–65] Contrary to microinjection alternatives where tip sizes are in the micrometer range, these nanoscale injection tools do not significantly deform the cellular or nuclear structure[63] or cause irreversible plasma membrane damage. This further allows for maintained insertion times within mammalian cell lines.[61,64] The NFPs used herein had tip radii on the order of 100 nm (Figure 1a inset). Additionally, injection of liquid solutions with the NFP requires less time to deliver a given dose than techniques that rely on release of adsorbed or bound doses,[62,64] a process that can require 30 min or more.[64] Thus the merits of the NFP for in vitro injection include nanoscale tip geometry for reduced invasiveness, rapid delivery of a broad range of functional agents in liquid solution, and the force and positional sensitivity of AFM control. Accordingly, we expect the NFP-based injection technique to be applicable to a host of nanomaterial-mediated drug delivery studies. Prospective studies involving the patterned injection of DNA-plasmids, siRNA, therapeutics, and conjugated NDs also have exciting implications in determining and directing cellular response.

4. Experimental Section

Agent-ND conjugation and characterization: DOX (Sigma-Aldrich, St. Louis, MO) and NDs (NanoCarbon Research Institute Ltd., Japan) were bound in accordance to a previous study.[3] Briefly, NDs were ultrasonicated at 100 W with a VWR 150D sonicator (VWR International, West Chester, PA) overnight and subsequently filtrated with Millex-GN 0.2-μm nylon filters (Millipore, Billerica, MA). The 5 mg mL^{-1} ND and 1 mg mL^{-1} DOX solution was then vortexed vigorously with a 2.3 μM NaOH solution. ND-PLL-FITC conjugates were fabricated in a similar way with 5 mg mL^{-1} ND and 0.5 mg mL^{-1} PLL-FITC (Invitrogen Corporation, Carlsbad, CA) within a 2.5 μM NaOH solution. They were then characterized against individual 5 mg mL^{-1} ND and 0.5 mg mL^{-1} PLL-FITC solutions via UV–Vis spectroscopy before and after spin-down (Beckman Coulter Microfuge 22R, Fullerton, CA) for 2 h at 14 000 rpm.

TEM characterization: ND-PLL-FITC samples were ultrasonicated for 5 min and immediately pipetted onto a commercial carbon TEM grid (Ted Pella Inc., Redding, CA). Upon air drying for 2 h, samples were then observed within a JEOL 2100F Field Emission TEM (JEOL Ltd., Peabody, MA) at high voltage (200 kV).

Nanofountain probe chips: NFP chips were fabricated as previously described.[71–73] To increase the reflectivity of the cantilevers for the AFM laser feedback, a 30-nm-thick layer of gold was sputtered (Denton Vacuum, Moorestown, NJ) on the backside of the chip. For each patterning or injection experiment, the NFP reservoirs were filled with $<$0.1 μL of the respective ND solution using a micropipette. This volume was sufficient to allow uninterrupted deposition for the duration of the experiments.

Nanodiamond patterning: DOX-ND dot arrays were patterned using the above solution on glass cover slips (Fisher Scientific, Pittsburgh, PA). Because the patterned arrays are not visible by optical microscopy, fiduciary markers were first created using a MTS Nano Indenter XP (MTS Systems Corp., Eden Prairie, MN) fitted with a Berkovich tip at an indentation force of 150 nN. During subsequent cell cultures, these fiduciary markers remained visible by optical microscopy such that the location of the patterned dot arrays was always known. The indented cover slips were sonicated for 5 min in deionized water and then ethanol prior to patterning. Contact angles between the DOX-ND solutions and substrate were measured using a VCA Optima surface analysis tool (AST Products, Billerica, MA).

Patterning experiments were conducted using a Veeco Instruments DI 3100 AFM (Plainview, NY) in constant force contact mode. The AFM was equipped with a 100-μm closed-loop xy-scanner from nPoint, Inc (Madison, WI). The resulting patterns were imaged and mapped relative to the fiduciary markers using the same Veeco AFM in tapping mode.

Cell culturing: MCF-7 human breast adenocarcinomas (ATCC, Manassas, VA), RAW 264.7 murine macrophages (ATCC, Manassas, VA), and RKO colorectal carcinomas (ATCC, Manassas, VA) were cultured in minimum essential Eagle medium (ATCC, Manassas, VA), Dulbecco's modification of Eagle's medium (Cellgro, Herndon, VA) and minimum essential medium (Hyclone, Logan, UT), respectively, all supplemented with 10% fetal bovine serum (ATCC, Manassas, VA) and 1% penicillin/streptomycin

small NANO MICRO

(Cambrex, East Rutherford, NJ) in an incubator at 37 °C and 5% CO_2.

TUNEL assay: RAW 264.7 murine macrophages (ATCC, Manassas, VA) were split at 80% confluency and 25 μL of this solution seeded upon the patterned and control substrates for 24 h for fluorescent TUNEL assay staining. Plain glass cover slips rinsed in deionized water and ethanol were used as substrates in the positive and negative controls. In the positive control, 2.5 $\mu g\,mL^{-1}$ of solubilized DOX was added to the media.

The TUNEL assay was completed in accordance with instructions and materials for adherent cultured cells provided by Chemicon International ApopTag Plus Fluorescein In situ Apoptosis Detection Kit S7111 (Temecula, CA). ApopTag utilizes the terminal deoxynucleotidyl transferase (TdT) enzyme to amplify the fluorescein-conjugated anti-digoxigenin antibody, a secondary antibody towards digoxigenin-labeled nucleotide-labeled 3′-OH termini on DNA fragments.

Fluorescence imaging: Fluorescence imaging was performed with a Nikon Eclipse ME600 microscope (Melville, NY) using a 100 W mercury lamp. Nikon LU Plan ELWD 50×/0.5 NA and LU Plan ELWD 100×/NA 0.8 objectives were used for cell and patterned DOX-ND imaging (Figure 2h,i), respectively. A Texas Red-HYQ filter set was used for counterstain imaging. A FITC-HYQ filter set was used for imaging fluorescein apoptotic signals (TUNEL positive) and DOX fluorescence. Images were captured in grayscale on a Jenoptik ProgRes CF^{COOL} (Germany) Peltier-cooled CCD camera using ProgRes CapturePro 2.5 software at 1360 × 1024 pixel resolution (24 bit depth). False color was applied to the images (532 nm for green, 620 nm for red) using the CapturePro software.

Direct nanodiamond injection: MCF-7 human breast adenocarcinoma cells, RAW 264.7 murine macrophages, and RKO colorectal carcinoma cells were cultured as described above. The same Veeco DI 3100 AFM was used for injection experiments. Immediately prior to NFP injection, extant media was temporarily aspirated such that only a thin meniscus of liquid remained covering the cells. The sample was then placed on the AFM stage and the optical microscope of the AFM used to locate the desired injection point. To perform the injection, the NFP was introduced to the cell with a force of 26 nN using the automatic approach function of the AFM for a prescribed time. Following injection, the sample was immediately removed, rinsed, and then submerged in phosphate buffer saline (PBS). Epi-fluorescent imaging was conducted with a FITC-HYQ filter as described above.

Acknowledgements

The authors acknowledge Dr. Shuyou Li of the Electron Probe Instrumentation Center (EPIC) at Northwestern University for obtaining TEM images and Dr. Eiji Osawa of the NanoCarbon Research Institute for his fruitful discussions. H.D.E. acknowledges the support provided by the Nanoscale Science and Engineering Initiative of the National Science Foundation (NSF) under NSF Award EEC-0647560 and the support provided by the NSF through Nanoscale Interdisciplinary Research Team Project CMS00304472. H.D.E. and O.L acknowledge use of the fabrication facilities of the Cornell University NanoScale Facility (Ithaca, NY), which is supported by NSF Grant ECS-0335765. D.H. gratefully acknowledges support from a V Foundation for Cancer Research V Scholars Award, National Science Foundation Center for Scalable and Integrated NanoManufacturing (SINAM) Grant DMI-0327077, Wallace H. Coulter Foundation Early Career Award in Translational Research, and National Institutes of Health grant U54 A1065359. O.L. and R.L. acknowledge the Northwestern Ryan Fellowship.

[1] P. Patel, D. Giljohann, D. Seferos, C. A. Mirkin, *Proc. Natl. Acad. Sci. USA* **2008**, *105*, 17222–17226.
[2] N. Rosi, D. Giljohann, C. Thaxton, A. Lytton-Jean, M. Han, C. A. Mirkin, *Science* **2006**, *312*, 1027–1030.
[3] H. Huang, E. Pierstorff, E. Osawa, D. Ho, *Nano Lett.* **2007**, *7*, 3305–3314.
[4] S. Gelperina, K. Kisich, M. Iseman, L. Heifets, *Am. J. Respir. Crit. Care Med.* **2005**, *172*, 1487–1490.
[5] T. Morgan, H. Muddana, E. Altinoglu, S. Rouse, A. Tabakovic, T. Tabouillot, T. Russin, S. Shanmugavelandy, P. Butler, P. Eklund, J. Yun, M. Kester, J. Adair, *Nano Lett.* **2008**, *8*, 4108–4115.
[6] O. Farokhzad, J. Cheng, B. Teply, I. Sherifi, S. Jon, P. Kantoff, J. Richie, R. Langer, *Proc. Natl. Acad. Sci. USA* **2006**, *103*, 6315–6320.
[7] E. Murphy, B. Majeti, L. Barnes, M. Makale, S. Weis, K. Lutu-Fuga, W. Wrasidlo, D. Cheresh, *Proc. Natl. Acad. Sci. USA* **2008**, *105*, 9343–9348.
[8] R. Lam, M. Chen, E. Pierstorff, H. Huang, E. Osawa, D. Ho, *ACS Nano* **2008**, *2*, 2095–2102.
[9] A. M. Schrand, H. Huang, C. Carlson, J. J. Schlager, E. Osawa, S. M. Hussain, L. Dai, *J. Phys. Chem. B* **2007**, *111*, 7353–7359.
[10] K. Bakowicz, S. Mitura, *J. Wide Bandgap Mater.* **2002**, *9*, 261–272.
[11] K. K. Liu, C. L. Cheng, C. C. Chang, J. I. Chao, *Nanotechnology* **2007**, *18*, 325102.
[12] A. M. Schrand, L. Dai, J. J. Schlager, S. M. Hussain, E. Osawa, *Diamond Relat. Mater.* **2007**, *16*, 2118–2123.
[13] R. Shukla, V. Bansal, M. Chaudhary, A. Basu, R. Bhonde, M. Sastry, *Langmuir* **2005**, *21*, 10644–10654.
[14] T. Tshikhudo, Z. Wang, M. Brust, *Mater. Sci. Technol.* **2004**, *20*, 980–984.
[15] M. Ozawa, M. Inaguma, M. Takahashi, F. Kataoka, A. Kruger, E. Osawa, *Adv. Mater.* **2007**, *19*, 1201–1206.
[16] V. Y. Dolmatov, *Uspekhi Khimii* **2001**, *70*, 687–708.
[17] A. Kruger, *Angew. Chem. Int. Ed.* **2006**, *45*, 6426–6427.
[18] W. S. Yeap, Y. Y. Tan, K. P. Loh, *Anal. Chem.* **2008**, *80*, 4659–4665.
[19] A. Kruger, Y. J. Liang, G. Jarre, J. Stegk, *J. Mater. Chem.* **2006**, *16*, 2322–2328.
[20] H. Huang, E. Pierstorff, E. Osawa, D. Ho, *ACS Nano* **2008**, *2*, 203–212.
[21] L. C. Huang, H. C. Chang, *Langmuir* **2004**, *20*, 5879–5884.
[22] K. Ushizawa, Y. Sato, T. Mitsumori, T. Machinami, T. Ueda, T. Ando, *Chem. Phys. Lett.* **2002**, *351*, 105–108.
[23] N. Kossovsky, A. Gelman, H. J. Hnatyszyn, S. Rajguru, R. L. Garrell, S. Torbati, S. S. F. Freitas, G. M. Chow, *Bioconjugate Chem.* **1995**, *6*, 507–511.
[24] A. Krueger, J. Stegk, Y. Liang, L. Lu, G. Jarre, *Langmuir* **2008**, *24*, 4200–4204.
[25] H. Huang, L. Dai, D. Wang, L.-S. Tan, E. Osawa, *J. Mater. Chem.* **2008**, *18*, 1347–1352.
[26] Y.-C. Chen, Y. Tzeng, A. Davray, A.-J. Cheng, R. Ramadoss, M. Park, *Diamond Relat. Mater.* **2008**, *17*, 722–727.
[27] Y.-C. Chen, Y. Tzeng, A.-J. Cheng, R. Dean, M. Park, B. Wilamowski, *Diamond Relat. Mater.* **2009**, *18*, 146–150.

[28] A. Ho, H. Espinosa, in *Applied Scanning Probe Methods 8: Scanning Probe Microscopy Techniques* (Eds: B. Bhushan, H. Fuchs, T. Masahiko) Springer, Heidelberg, Germany **2008**.
[29] D. Prime, S. Paul, C. Pearson, M. Green, M. Petty, *Mater. Sci. Eng. C* **2004**, *25*, 33–38.
[30] D. Roy, M. Munz, P. Colombi, S. Bhattacharyya, J.-P. Salvetat, P. Cumpson, M.-L. Saboungi, *Appl. Surf. Sci.* **2007**, *254*, 1394–1398.
[31] W. Wang, R. Stoltenberg, S. Liu, Z. Bao, *ACS Nano* **2008**, *2*, 2135–2142.
[32] B. Wu, A. Ho, N. Moldovan, H. D. Espinosa, *Langmuir* **2007**, *23*, 9120–9123.
[33] V. Santhanam, R. Andres, *Nano Lett.* **2004**, *4*, 41–44.
[34] X. Wu, L. Chi, H. Fuchs, *Eur. J. Inorg. Chem.* **2005**, 3729–3733.
[35] T. Kraus, L. Malaquin, H. Schmid, W. Riess, N. Spencer, H. Wolf, *Nat. Nanotechnol.* **2007**, *2*, 570–576.
[36] J.-U. Park, M. Hardy, S. Kang, K. Barton, K. Adair, D. Mukhopadhyay, C. Lee, M. Strano, A. Alleyne, J. Georgiadis, P. Ferreira, J. Rogers, *Nature* **2007**, *6*, 782–789.
[37] K. Murata, J. Matsumoto, A. Tezuka, Y. Matsuba, H. Yokoyama, *Microsyst. Technol.* **2005**, *12*, 2–7.
[38] F. Iwata, S. Nagami, Y. Sumiya, A. Sasaki, *Nanotechnology* **2007**, *18*, 105301.
[39] E. Duoss, M. Twardowski, J. Lewis, *Adv. Mater.* **2007**, *19*, 3485–3489.
[40] K.-J. Jang, J.-M. Nam, *Small* **2008**, *4*, 1930–1935.
[41] S. Vengasandra, M. Lynch, J. Xu, E. Henderson, *Nanotechnology* **2005**, *16*, 2052–2055.
[42] D. Harris, H. Hu, J. Conrad, J. Lewis, *Phys. Rev. Lett.* **2007**, *98*, 148301.
[43] R. Shepherd, P. Panda, Z. Bao, K. Sandhage, T. Hatton, J. Lewis, P. Doyle, *Adv. Mater.* **2008**, *20*, 4734–4739.
[44] X. Liu, L. Fu, S. Hong, V. Dravid, C. A. Mirkin, *Adv. Mater.* **2002**, *14*, 231–234.
[45] L. Demers, S.-J. Park, T. Taton, Z. Li, C. A. Mirkin, *Angew. Chem. Int. Ed.* **2001**, *40*, 3071–3073.
[46] R. D. Piner, J. Zhu, F. Xu, S. H. Hong, C. A. Mirkin, *Science* **1999**, *283*, 661–663.
[47] K. Salaita, Y. Wang, C. A. Mirkin, *Nat. Nanotechnol.* **2007**, *2*, 145–155.
[48] P. Mendes, S. Jacke, K. Critchley, J. Plaza, Y. Chen, K. Nikitin, R. Palmer, J. Preece, S. Evans, D. Fitzmaurice, *Langmuir* **2004**, *20*, 3766–3768.
[49] S.-S. Bae, D. Lim, J.-I. Park, W.-R. Lee, J. Cheon, S. Kim, *J. Phys. Chem. B* **2004**, *108*, 2575–2579.
[50] M. Zin, H. Ma, M. Sarikaya, A. Jen, *Small* **2005**, *1*, 698–702.
[51] G. Gregoriadis, R. A. Buckland, *Nature* **1973**, *244*, 170–172.
[52] S. R. Schwarze, K. A. Hruska, S. F. Dowdy, *Trends Cell Biol.* **2000**, *10*, 290–295.
[53] T. Uchida, M. Yamaizumi, Y. Okada, *Nature* **1977**, *266*, 839–840.
[54] F. L. Graham, A. J. van der Eb, *Virology* **1973**, *52*, 456–467.
[55] G. Chu, P. A. Sharp, *Gene* **1981**, *13*, 197–202.
[56] D. E. Knight, M. C. Scrutton, *Biochem. J.* **1986**, *234*, 497–506.
[57] J. Eul, M. Graessmann, A. Graessmann, *FEBS Lett.* **1996**, *394*, 227–232.
[58] J. E. Celis, *Biochem. J.* **1984**, *223*, 281–291.
[59] R. Pepperkok, J. Scheel, H. Horstmann, H. P. Hauri, G. Griffiths, T. E. Kreis, *Cell* **1993**, *74*, 71–82.
[60] D. J. Stephens, R. Pepperkok, *Proc. Natl. Acad. Sci. USA* **2001**, *98*, 4295–4298.
[61] S. Han, C. Nakamura, I. Obataya, N. Nakamura, J. Miyake, *Biochem. Biophys. Res. Commun.* **2005**, *332*, 633–639.
[62] S.-W. Han, C. Nakamura, N. Kotobuki, I. Obataya, H. Ohgushi, T. Nagamune, J. Miyake, *Nanomedicine* **2008**, *4*, 215–225.
[63] I. Obataya, C. Nakamura, S. W. Han, N. Nakamura, J. Miyake, *Nano Lett.* **2005**, *5*, 27–30.
[64] X. Chen, A. Kis, A. Zettl, C. R. Bertozzi, *Proc. Natl. Acad. Sci. USA* **2007**, *104*, 8218–8222.
[65] M. Knoblauch, J. M. Hibberd, J. C. Gray, A. J. E. van Bel, *Nat. Biotechnol.* **1999**, *17*, 906–909.
[66] T. Tsulaia, N. Prokopishyn, A. Yao, N. Victor Carsrud, M. Clara Carou, D. Brown, B. Davis, J. Yannariello-Brown, *J. Biomed. Sci.* **2003**, *10*, 328–336.
[67] C. M. Cuerrier, R. Lebel, M. Grandbois, *Biochem. Biophys. Res. Commun.* **2007**, *355*, 632–636.
[68] P. Belaubre, M. Guirardel, G. Garcia, J. B. Pourciel, V. Leberre, A. Dagkessamanskaia, E. Trevisiol, J. M. Francois, C. Bergaud, *Appl. Phys. Lett.* **2003**, *82*, 3122–3124.
[69] F. Stracke, I. Rieman, K. König, *J. Photochem. Photobiol. B* **2005**, *81*, 136–142.
[70] F. O. Laforge, J. Carpino, S. A. Rotenberg, M. V. Mirkin, *Proc. Natl. Acad. Sci. USA* **2007**, *104*, 11895–11900.
[71] K. H. Kim, N. Moldovan, H. D. Espinosa, *Small* **2005**, *1*, 632–635.
[72] N. Moldovan, K. H. Kim, H. D. Espinosa, *J. Microelectromech. Syst.* **2006**, *15*, 204–213.
[73] N. Moldovan, K.-H. Kim, H. D. Espinosa, *J. Micromech. Microeng.* **2006**, *16*, 1935–1942.
[74] O. Loh, A. Ho, J. Rim, P. Kohli, N. Patankar, H. Espinosa, *Proc. Natl. Acad. Sci. USA* **2008**, *105*, 16438–16443.
[75] K.-H. Kim, R. G. Sanedrin, A. M. Ho, S. W. Lee, N. Moldovan, C. A. Mirkin, H. D. Espinosa, *Adv. Mater.* **2008**, *20*, 330–334.
[76] G. Kong, G. Anyarambhatla, W. Petros, R. Braun, O. Colvin, D. Needham, M. Dewhirst, *Cancer Res.* **2000**, *60*, 6950–6957.
[77] X. Dai, Z. Yue, M. Eccleston, J. Swartling, N. Slater, C. Kaminski, *Nanomedicine* **2008**, *4*, 49–56.
[78] Y. Gavrieli, Y. Sherman, S. Ben-Sasson, *J. Cell Biol.* **1992**, *119*, 493–501.
[79] C.-C. Fu, H.-Y. Lee, K. Chen, T.-S. Lim, H.-Y. Wu, P.-K. Lin, P.-K. Wei, P.-H. Tsao, H.-C. Chang, W. Fann, *Proc. Natl. Acad. Sci. USA* **2007**, *104*, 727–732.
[80] L. C. Huang, H. C. Chang, *Langmuir* **2004**, *20*, 5879–5884.
[81] X. L. Kong, L. C. L. Huang, C. M. Hsu, W. H. Chen, C. C. Han, H. C. Chang, *Anal. Chem.* **2005**, *77*, 259–265.
[82] C. Nicholson, L. Tao, *Biophys. J.* **1993**, *65*, 2277–2290.
[83] R. Thorne, C. Nicholson, *Proc. Natl. Acad. Sci. USA* **2006**, *103*, 5567–5572.
[84] Y.-R. Chang, H.-Y. Lee, K. Chen, C.-C. Chang, D.-S. Tsai, C.-C. Fu, T.-S. Lim, Y.-K. Tzeng, C.-Y. Fang, C.-C. Han, H.-C. Chang, W. Fann, *Nat. Nanotechnol.* **2008**, *3*, 284–288.
[85] G. Lukacs, P. Haggie, O. Seksek, D. Lechardeur, N. Freedman, A. Verkman, *J. Biol. Chem.* **2000**, *275*, 1625–1629.
[86] N. Fatin-Rouge, K. Starchev, J. Buffle, *Biophys. J.* **2004**, *86*, 2710–2719.
[87] W. Jiang, K. Betty, J. Rutka, W. Chan, *Nat. Nanotechnol.* **2008**, *3*, 145–150.
[88] K.-J. Jang, J.-M. Nam, *Small* **2008**, *4*, 1930–1935.
[89] D. Guerin, S. Ismat Shah, *J. Mater. Sci. Lett.* **1997**, *16*, 476–478.
[90] Y. Lifshitz, C. H. Lee, Y. Wu, W. J. Zhang, I. Bello, S. T. Lee, *Appl. Phys. Lett.* **2006**, *88*, 243114.

Received: March 1, 2009
Revised: April 9, 2009
Published online: May 12, 2009

